JOURNAL OF GUIDANCE, CONTROL, AND DYNAMICS
Vol. 34, No. 2, March–April 2011

Fuel Optimization for Continuous-Thrust Orbital Rendezvous with Collision Avoidance Constraint

Richard Epenoy*
Centre National d'Etudes Spatiales, 31401 Toulouse, France

DOI: 10.2514/1.50996

This paper focuses on the issue of minimum-fuel rendezvous between an active chaser satellite with continuous-thrust capability and a passive target satellite. It is first formalized as an optimal control problem subject to a collision-avoidance constraint on the path of the chaser satellite. Then, a new method for dealing with this state constraint is built by adapting to the optimal control framework a recently developed approach for solving inequality-constrained nonlinear programming problems. The resulting method implies solving a sequence of unconstrained optimal control problems, the solutions of which converge toward the solution of the original problem. Convergence of the method is proved, and its efficiency is demonstrated through numerical results obtained in the case of a rendezvous in a highly elliptical orbit.

I. Introduction

IN THE field of space trajectory design, the optimization of rendezvous trajectories is a key problem that arises in different space applications. Formation flying missions such as PROBA-3 [1], the demonstration mission of the ESA, or PRISMA [2], a technology mission of the Swedish Space Corporation, involve multiple rendezvous phases. For example, for each of the formation reconfiguration maneuvers, fuel-optimal trajectories must be found that avoid collisions between the satellites. Other rendezvous problems arise from servicing missions to the International Space Station, such as with ESA's automated transfer vehicle [3], or from exploration missions in Mars orbit [4]. New mission concepts such as SMART-OLEV [5], which is dedicated to the refueling of geostationary satellites, are also in need of rendezvous strategies.

Direct transcription methods are often used for solving optimal control problems in the context of rendezvous trajectories. These methods discretize the time horizon and the control and state variables. The optimal control and the state discrete values are then computed using a numerical optimization method that is either deterministic [6–8] or heuristic, such as genetic algorithms or multiagent optimization [9–12]. These approaches are efficient, and they handle additional state constraints such as collision-avoidance requirements [7,8,13–16]. In [17–19], a mixed-integer linear programming methodology is developed for this purpose. In [20], Louembet et al. combined a direct transcription method with the differential flatness concept in order to arrive at a linear matrix inequality problem that they then solved, thanks to an adapted algorithm.

When no state constraint exists, some authors have solved minimum-fuel problems by directly using the Pontryagin's maximum principle (PMP) [21,22]. This approach leads to a two-point boundary value problem (TPBVP) that is then solved by means of shooting methods [23]. For example, Beard et al. [24] used this approach for the optimal rotation of spacecraft formations, and Thevenet and Epenoy [25] applied it to the deployment of formations.

Few authors have used the PMP to try to solve the inequality state-constrained optimal control problem that arises when a collision-avoidance constraint is imposed on a continuous-thrust rendezvous. Kim et al. [26] assumed a particular structure of the optimal trajectory in terms of the unconstrained and state-constrained arcs. Then, they numerically determined when to switch from one arc to another by solving a multipoint boundary value problem (MPBVP).

In the case of inequality state constraints, the PMP takes a complex mathematical form that is not directly tractable from a numerical point of view [27]. The main issue is that the structure of the optimal trajectory must be guessed a priori. Key questions are as follows:

1) How many times is a state constraint active, i.e., verified as an equality, during the time horizon?

2) Is a state constraint active at isolated points, called contact points, or during nonzero time intervals?

Depending on the answers to these questions, the resulting MPBVP may take very different forms. To circumvent this difficulty, some authors penalized state constraints violations by introducing an additional term in the cost function [28–30]. These common penalization approaches suffer from known drawbacks. They are difficult to tune, appear to not always be efficient on actual optimal control problems, and their convergence is not necessarily guaranteed. In the particular case of mixed control-state constraints, Graichen and Petit [31] proposed the use of saturation functions. A homotopy algorithm has also been developed by Hermant [32] for dealing with second-order state constraints. This last approach seems difficult to use in practice, as it requires the management of different formulations of the PMP during the course of the algorithm. Indeed, the structure of the trajectory depends on the homotopy parameter.

In the mathematical programming field, exact penalty functions are well known [33] and allow the transformation of a constrained problem into an equivalent unconstrained one. Their major drawback is that they are, in general, not differentiable and thus lead to a nondifferentiable unconstrained problem. This last one can be solved either by means of subgradient methods (only if the problem is convex) or by using derivative-free algorithms. To make the problem differentiable, some authors tried to smoothen exact penalty functions [34–37] while preserving their interesting properties. In this paper, an algorithm for solving the minimum-fuel rendezvous problem with collision-avoidance constraint is built by adapting the recent approach developed by Liuzzi and Lucidi [37]. Thus, it will be shown that it is possible to efficiently solve this kind of optimal control problem simply by solving a sequence of TPBVPs, without any a priori knowledge on the structure of the optimal trajectory.

The use of exact penalty functions is not new in optimal control. For example, Smith and Mayne [38] and Mayne and Polak [39,40] used the same idea for dealing with control and terminal equality constraints. However, this is the first time that smoothed exact penalty functions [34–37] are applied to the solution of inequality state-constrained optimal control problems for ordinary differential equations.

Received 1 June 2010; revision received 21 October 2010; accepted for publication 21 October 2010.

*Research Engineer, Orbital Maneuvers Department, 18 Avenue Edouard Belin, Cedex 9; Richard.Epenoy@cnes.fr.

This paper is organized as follows. In Sec. II, notations are defined and the state-constrained minimum-fuel rendezvous problem is formulated. The solution of its unconstrained counterpart is also investigated. The main theoretical and practical features of the method are developed in Sec. III. In Sec. IV, the efficiency of the method is illustrated through numerical results obtained in the case of a rendezvous in highly elliptical orbits (HEOs). Conclusions are drawn in Sec. V. The Appendix presents the convergence proof of the method developed in Sec. III.

II. Problem Statement

Consider a chaser satellite equipped with a continuous-thrust propulsion system and a passive target satellite, both flying on elliptical orbits. Assume, in addition, that there is no orbital perturbation; that is, the motions of the two vehicles are Keplerian. Finally, suppose that the distance between the two satellites remains small compared with the distance between the target satellite and the Earth's center of mass. Then, the relative motion of the chaser with respect to the target can be described by Tschauner–Hempel equations [41,42].

A. Dynamical Equations

Consider Hill's local orbital frame centered on the target satellite and denoted as $(\boldsymbol{R}, \boldsymbol{S}, \boldsymbol{W})$.

In addition, let a, $e \in [0, 1)$, and v denote, respectively, the semimajor axis, the eccentricity, and the true anomaly of the target satellite and let μ designate the Earth's gravitational constant. Moreover, let $X(t)$, $Y(t)$, and $Z(t)$ be the coordinates of the chaser in the preceding local orbital frame at a given date t, and let $\tilde{X}(v)$, $\tilde{Y}(v)$, and $\tilde{Z}(v)$ be the same coordinates but considered as functions of v.

Now, let $x_1(v)$, $x_2(v)$, and $x_3(v)$ be defined as follows:

$$\begin{bmatrix} x_1(v) \\ x_2(v) \\ x_3(v) \end{bmatrix} = [1 + e\cos(v)] \begin{bmatrix} \tilde{X}(v) \\ \tilde{Y}(v) \\ \tilde{Z}(v) \end{bmatrix} \tag{1}$$

and let $x_4(v)$, $x_5(v)$, and $x_6(v)$ be their corresponding first derivatives with respect to v.

In the following, $m(v)$ will stand for the mass of the chaser at the true anomaly v. Moreover, $F_{\max}$ and $I\mathrm{sp}$ will denote the maximum thrust modulus and the specific impulse of the chaser's engine. In addition, $\boldsymbol{u}(v) \in \Re^3$ will be the normalized thrust vector of the chaser at the true anomaly v, expressed in the $(\boldsymbol{R}, \boldsymbol{S}, \boldsymbol{W})$ frame. This vector will satisfy $\|\boldsymbol{u}(v)\| \le 1$, where $\|\cdot\|$ denotes the Euclidian norm. Finally, $g_0 = 9.80665\ \mathrm{m\,s^{-2}}$ will denote the acceleration due to gravity at sea level.

With the preceding notations, Tschauner–Hempel equations [41,42] can be written as follows:

$$\begin{cases} \dot{\boldsymbol{x}}(v) = \boldsymbol{A}(v)\boldsymbol{x}(v) + \boldsymbol{B}(v)\frac{\boldsymbol{u}(v)}{m(v)} \\ \dot{m}(v) = -c(v)\|\boldsymbol{u}(v)\| \end{cases} \tag{2}$$

where

$$\boldsymbol{x}(v) = \begin{pmatrix} x_1(v) \\ \vdots \\ x_6(v) \end{pmatrix}; \quad \boldsymbol{A}(v) = \begin{bmatrix} 0 & 0 & 0 & 1 & 0 & 0 \\ 0 & 0 & 0 & 0 & 1 & 0 \\ 0 & 0 & 0 & 0 & 0 & 1 \\ a(v) & 0 & 0 & 0 & 2 & 0 \\ 0 & 0 & 0 & -2 & 0 & 0 \\ 0 & 0 & -1 & 0 & 0 & 0 \end{bmatrix}$$
$$\boldsymbol{B}(v) = b(v) \begin{bmatrix} 0 & 0 & 0 \\ 0 & 0 & 0 \\ 0 & 0 & 0 \\ 1 & 0 & 0 \\ 0 & 1 & 0 \\ 0 & 0 & 1 \end{bmatrix} \tag{3}$$

with

$$a(v) = \frac{3}{[1 + e\cos(v)]}; \qquad b(v) = \frac{a^3(1 - e^2)^3}{[1 + e\cos(v)]^3}\frac{F_{\max}}{\mu}$$
$$c(v) = \frac{a^{3/2}(1 - e^2)^{3/2}}{[1 + e\cos(v)]^2}\frac{F_{\max}}{\sqrt{\mu}g_0 I\mathrm{sp}} \tag{4}$$

B. State-Constrained Optimal Control Problem

Assuming that the initial and final anomalies (denoted, respectively, as v_0 and v_f) are fixed, with $v_0 < v_f$, it is now possible to write the minimum-fuel optimal control problem, denoted as (P), as follows:

Find

$$\bar{\boldsymbol{u}} = \arg\min_u J(\boldsymbol{u}) = -m(v_f) \tag{5}$$

such that

$$\begin{aligned} &\dot{\boldsymbol{x}}(v) = \boldsymbol{A}(v)\boldsymbol{x}(v) + \boldsymbol{B}(v)\frac{\boldsymbol{u}(v)}{m(v)} \\ &\dot{m}(v) = -c(v)\|\boldsymbol{u}(v)\| \\ &\|\boldsymbol{u}(v)\| \le 1, \qquad v \in [v_0, v_f] \\ &g[v, \boldsymbol{x}(v)] \le 0, \qquad v \in [v_0, v_f] \\ &\boldsymbol{x}(v_0) = \boldsymbol{x}_0, \qquad h[\boldsymbol{x}(v_f)] = \boldsymbol{0} \\ &m(v_0) = m_0 \end{aligned}$$

It is assumed here that the initial mass of the chaser $m_0 > 0$ is given. The initial vector $\boldsymbol{x}_0$ in Eq. (5) is fixed and can be computed from the original relative position and velocity (time derivatives) vectors of the chaser. The terminal conditions are defined thanks to function $h(.)$. This formulation encompasses the case where all the components of $\boldsymbol{x}(v_f)$ are fixed at the final anomaly v_f. In this case, $h(.)$ takes the form $h[\boldsymbol{x}(v_f)] = \boldsymbol{x}(v_f) - \boldsymbol{x}_f$ for a fixed vector $\boldsymbol{x}_f$. The formulation allows the coverage of more complex cases, where the final conditions correspond to a stable relative orbit around the target satellite, as in [43].

Finally, by using Eq. (1), the state constraint in Eq. (5) can be written in the following form:

$$g[v, \boldsymbol{x}(v)] = 1 - \frac{\sqrt{x_1^2(v) + x_2^2(v) + x_3^2(v)}}{d_{\min}[1 + e\cos(v)]} \le 0; \qquad v \in [v_0, v_f] \tag{6}$$

where $d_{\min} > 0$ denotes the minimum safety distance required between the chaser satellite and the target satellite.

In the following, (P^0) will designate the unconstrained problem obtained by dropping the state constraint in Eq. (6) from Eq. (5). It will be assumed that (P^0) has a solution denoted as $\boldsymbol{u}^0$ and associated with the optimal states $\boldsymbol{x}^0$ and m^0. In addition, the solution $\bar{\boldsymbol{u}}$ of problem (P) corresponds to optimal states denoted as $\bar{\boldsymbol{x}}$ and $\bar{m}$.

C. Solving the Unconstrained Problem

Even if problem (P^0) is easier to solve than problem (P), its solution through the PMP is not straightforward. Indeed, it will be shown next that the optimal control $\boldsymbol{u}^0(\cdot)$ has a bang-off-bang structure. Then, according to [44], the shooting function arising from the PMP is not continuously differentiable, and its Jacobian is singular on a large domain. As a consequence, solving problem (P^0) by means of shooting methods is very difficult. A regularization technique has been developed in [44] for solving this kind of minimum-fuel problem. The same technique was used in [25], and it will be applied again here to the solution of problem (P^0).

Following [44], a regularized state constraint-free problem, denoted as $(P^0)_\delta$, is established as follows:

Find

$$\boldsymbol{u}_\delta^0 = \arg\min_u J_\delta(\boldsymbol{u}) = -m(v_f) - \delta\int_{v_0}^{v_f} F[v, \boldsymbol{u}(v)]\,\mathrm{d}v \tag{7}$$

such that

$$\begin{aligned}
&\dot{\boldsymbol{x}}(v) = \boldsymbol{A}(v)\boldsymbol{x}(v) + \boldsymbol{B}(v)\frac{\boldsymbol{u}(v)}{m(v)}\\
&\dot{m}(v) = -c(v)\|\boldsymbol{u}(v)\|\\
&\|\boldsymbol{u}(v)\| \leq 1, \qquad v \in [v_0, v_f]\\
&\boldsymbol{x}(v_0) = x_0, \qquad h[\boldsymbol{x}(v_f)] = \boldsymbol{0}\\
&m(v_0) = m_0
\end{aligned}$$

where $\delta \geq 0$, and where function $F(\cdots, \cdots)$ is given hereafter as

$$F[v, \boldsymbol{u}(v)] = c(v)(\log(\|\boldsymbol{u}(v)\|) + \log[1 - \|\boldsymbol{u}(v)\|]) \qquad v \in [v_0, v_f] \tag{8}$$

For a given $n > 0$, a sequence of values denoted as $(\delta)_i$ $(i = 1, \ldots, n)$ is defined with $(\delta_1 > \delta_2 > \cdots > \delta_n > 0)$. Then, problems $(P^0)_{\delta_i}$ $(i = 2, \ldots, n)$ are successively solved by using the solution obtained at step $(i-1)$ as an initial guess for step i {see [44] for more details about how to solve the first problem $(P^0)_{\delta_1}$}. Finally, assuming that δ_n is sufficiently small, the solution of $(P^0)_{\delta_n}$ provides a very accurate approximation of the solution of (P^0) (see [44]).

In the following, the optimal states associated with $\boldsymbol{u}_\delta^0$ will be denoted by $\boldsymbol{x}_\delta^0$ and m_δ^0. Moreover, $\boldsymbol{p}_x$ and p_m will designate, respectively, the costate vector associated with the state $\boldsymbol{x}_\delta^0$ and the costate associated with m_δ^0. Finally, the standard superscript T will denote the transpose operator.

According to the PMP [21,22], the optimal control $\boldsymbol{u}_\delta^0(v)$ takes the following form when $\boldsymbol{B}(v)^T\boldsymbol{p}_x(v) \neq \boldsymbol{0}$:

$$\boldsymbol{u}_\delta^0(v) = -\beta_\delta^0(v)\frac{\boldsymbol{B}(v)^T\boldsymbol{p}_x(v)}{\|\boldsymbol{B}(v)^T\boldsymbol{p}_x(v)\|} \tag{9}$$

with

$$\begin{aligned}
\beta_\delta^0(v) &= \frac{2\delta}{2\delta - \rho(v) + \sqrt{\rho(v)^2 + 4\delta^2}}\\
\rho(v) &= p_m(v) + \frac{\|\boldsymbol{B}(v)^T\boldsymbol{p}_x(v)\|}{m(v)c(v)}
\end{aligned} \tag{10}$$

In the particular case where $\boldsymbol{B}(v)^T\boldsymbol{p}_x(v) = \boldsymbol{0}$, the thrust direction is undetermined, and Eq. (9) reduces to

$$\|\boldsymbol{u}_\delta^0(v)\| = \beta_\delta^0(v) \tag{11}$$

Then, in both cases, the following holds:

$$\|\boldsymbol{u}_\delta^0(v)\| \in (0, 1); \qquad v \in [v_0, v_f] \tag{12}$$

The key point in [44] is that $\boldsymbol{u}_\delta^0(\cdot)$ is a smooth approximation of the bang-off-bang optimal control $\boldsymbol{u}^0(\cdot)$.

Indeed, denoting again for convenience by $\boldsymbol{p}_x$ and p_m (the costates associated, respectively, with $\boldsymbol{x}^0$ and m^0), $\boldsymbol{u}^0(v)$ can be written as follows when $\boldsymbol{B}(v)^T\boldsymbol{p}_x(v) \neq \boldsymbol{0}$:

$$\boldsymbol{u}^0(v) = -\beta^0(v)\frac{\boldsymbol{B}(v)^T\boldsymbol{p}_x(v)}{\|\boldsymbol{B}(v)^T\boldsymbol{p}_x(v)\|} \tag{13}$$

with

$$\beta^0(v) = \begin{cases} 0 & \text{if } \rho(v) < 0\\ 1 & \text{if } \rho(v) > 0\\ w \in [0, 1] & \text{if } \rho(v) = 0 \end{cases} \tag{14}$$

where $\rho(v)$ is defined in Eq. (10). Thus, assuming that no singular arc exists [21,22], the interval $[v_0, v_f]$ splits into subintervals on which alternately $\beta^0(v) = 1$ (the engine is on) and $\beta^0(v) = 0$ (the engine is off). This is why the control $\boldsymbol{u}^0(\cdot)$ is said to be bang-off-bang.

In the particular case where $\boldsymbol{B}(v)^T\boldsymbol{p}_x(v) = \boldsymbol{0}$, the following holds:

$$\|\boldsymbol{u}^0(v)\| = \beta^0(v) \tag{15}$$

It is easy to deduce from Eqs. (10) and (14) that $\beta_\delta^0(v)$ (considered as a function of $\rho(v)$) is a smooth approximation of $\beta^0(v)$ that converges toward $\beta^0(v)$ as δ tends to zero [44]. Then, $\beta_\delta^0(\cdot)$ presents sharp variations in the vicinity of some points when δ is close to zero.

In addition, the costates equations for $(P^0)_\delta$ and (P^0) take the same following form:

$$\begin{cases} \dot{\boldsymbol{p}}_x(v) = -\boldsymbol{A}(v)^T\boldsymbol{p}_x(v)\\ \dot{p}_m(v) = -\beta(v)\frac{\|\boldsymbol{B}(v)^T\boldsymbol{p}_x(v)\|}{m^2(v)} \end{cases} \tag{16}$$

where $\beta(v) = \beta_\delta^0(v)$ [see Eq. (10)] for problem $(P^0)_\delta$ and $\beta(v) = \beta^0(v)$ [see Eq. (14)] for problem (P^0).

Finally, the transversality conditions given by the PMP lead here, for both problems, to

$$\begin{cases} \boldsymbol{p}_x(v_f) = \left[\frac{\partial h[\boldsymbol{x}(v_f)]}{\partial \boldsymbol{x}}\right]^{\boldsymbol{T}}\boldsymbol{\chi}\\ p_m(v_f) = -1 \end{cases} \tag{17}$$

where $\boldsymbol{\chi} \in \Re^{n_h}$, if $h(.)\colon \Re^6 \to \Re^{n_h}$ with $n_h > 0$.

D. Smoothed State-Constrained Problem $(P)_{\delta_n}$

Once the solution of problem (P^0) has been obtained by using the technique developed in [44], it is possible to solve problem (P) by adapting the ideas given in [37] to the optimal control framework. But first, as for problem (P^0), it is necessary to introduce a logarithmic barrier term depending on v and $\boldsymbol{u}(v)$ in the performance index of problem (P). The goal is to again smoothen the control law and to avoid numerical difficulties.

With this aim in view, consider the following regularized state-constrained problem, denoted as $(P)_{\delta_n}$:

Find

$$\bar{\boldsymbol{u}}_{\delta_n} = \arg\min_u, \ J_{\delta_n}(\boldsymbol{u}) = -m(v_f) - \delta_n\int_{v_0}^{v_f} F[v, \boldsymbol{u}(v)]\,\mathrm{d}v \tag{18}$$

such that

$$\begin{aligned}
&\dot{\boldsymbol{x}}(v) = \boldsymbol{A}(v)\boldsymbol{x}(v) + \boldsymbol{B}(v)\frac{\boldsymbol{u}(v)}{m(v)}\\
&\dot{m}(v) = -c(v)\|\boldsymbol{u}(v)\|\\
&\|\boldsymbol{u}(v)\| \leq 1, \qquad v \in [v_0, v_f]\\
&g[v, \boldsymbol{x}(v)] \leq 0, \qquad v \in [v_0, v_f]\\
&\boldsymbol{x}(v_0) = \boldsymbol{x}_0, \qquad h[\boldsymbol{x}(v_f)] = \boldsymbol{0}\\
&m(v_0) = m_0
\end{aligned}$$

where function $F(\cdots, \cdots)$ is defined in Eq. (8) and where δ_n is the last value in the sequence of parameters $(\delta_i)_{i=1,\ldots,n}$ used for solving Eq. (7).

In the following, the optimal states associated with $\bar{\boldsymbol{u}}_{\delta_n}$ will be denoted by $\bar{\boldsymbol{x}}_{\delta_n}$ and $\bar{m}_{\delta_n}$. As δ_n is assumed to be small, these states are very close to the corresponding ones of Eq. (5) [44]. Moreover, the control $\bar{\boldsymbol{u}}_{\delta_n}(.)$ is smooth, but it is very close to the bang-off-bang control $\bar{\boldsymbol{u}}(.)$ [44]. Indeed, $\bar{\boldsymbol{u}}_{\delta_n}$ depends on its associated states, $\bar{\boldsymbol{x}}_{\delta_n}$ and $\bar{m}_{\delta_n}$, and costates (denoted here again for convenience by $\boldsymbol{p}_x$ and p_m) through Eqs. (9–11) with $\delta = \delta_n$, where $\boldsymbol{u}_\delta^0(v)$ and $\beta_\delta^0(v)$ are replaced, respectively, by $\bar{\boldsymbol{u}}_{\delta_n}(v)$ and a new term denoted as $\bar{\beta}_{\delta_n}(v)$.

The transversality conditions for Eq. (18) are still given by Eq. (17). The costates equations of Eq. (18) are as complex as those of Eq. (5) (see [27]) due to the presence of the state constraint in Eq. (6). Indeed, they depend on the structure of the optimal trajectory that is not known a priori.

Finally, the following condition equivalent to Eq. (12) is satisfied by $\bar{\boldsymbol{u}}_{\delta_n}(.)$

$$\|\bar{\boldsymbol{u}}_{\delta_n}(v)\| \in (0,1); \qquad v \in [v_0, v_f] \tag{19}$$

III. New Approach for Dealing with State Constraint

A. Introduction

Let $\alpha > 0$, $\sigma > 0$, and $\varepsilon > 0$ be given. Then, consider the two following functions:

$$\forall\ z \in (-\infty, \alpha); \qquad \varphi_{\alpha,\varepsilon}(z) = \max\left[0, \quad \frac{z}{\varepsilon}\left(1 + \frac{\varepsilon}{\alpha - z}\right)\right] \tag{20}$$

$$\forall\ z \in (-\infty, \alpha);$$
$$\psi_{\sigma,\alpha,\varepsilon}(z) = \sigma \log\left\{1 + \exp\left[\frac{z}{\sigma\varepsilon}\left(1 + \frac{\varepsilon}{\alpha - z}\right)\right]\right\} \tag{21}$$

In [37], the function in Eq. (20) is used to build an exact penalty function for inequality constrained mathematical programming problems when ε and α are sufficiently small. The function in Eq. (21) is a smooth approximation of the function in Eq. (20) that tends to this last one as $\sigma \to 0$. These two functions have interesting properties given hereafter.

Lemma 1: Let $\alpha > 0$, $\sigma > 0$, and $\varepsilon > 0$ be given. Then, the following holds:

$$\forall\ z \in (-\infty, \alpha); \qquad \varphi_{\alpha,\varepsilon}(z) < \psi_{\sigma,\alpha,\varepsilon}(z) < \varphi_{\alpha,\varepsilon}(z) + \sigma \log(2)$$

Proof: See [37] for example. □

Lemma 2: Let $\alpha > 0$, $z \in (-\infty, \alpha)$, and $\varepsilon > 0$ be given. Then, function $[\sigma \to \Psi(\sigma) = \psi_{\sigma,\alpha,\varepsilon}(z)]$ is strictly increasing on $(0, +\infty)$.

Proof: For $\sigma > 0$, let $w_{\sigma,\alpha,\varepsilon}(z)$ be defined by

$$w_{\sigma,\alpha,\varepsilon}(z) = \frac{z}{\sigma\varepsilon}\left(1 + \frac{\varepsilon}{\alpha - z}\right) \tag{22}$$

Then, the following holds:

$$\Psi'(\sigma) = \frac{\{1 + \exp[w_{\sigma,\alpha,\varepsilon}(z)]\}\log\{1 + \exp[w_{\sigma,\alpha,\varepsilon}(z)]\} - w_{\sigma,\alpha,\varepsilon}(z)\exp[w_{\sigma,\alpha,\varepsilon}(z)]}{1 + \exp[w_{\sigma,\alpha,\varepsilon}(z)]} > 0$$

□

Lemma 3: Let $z \in (-\infty, 0)$, $\varepsilon > 0$, and $\sigma > 0$ be given. Then, function $[\alpha \to \Omega(\alpha) = \psi_{\sigma,\alpha,\varepsilon}(z)]$ is strictly increasing on $(0, +\infty)$.

Proof: For $\alpha > 0$, the following holds:

$$\Omega'(\alpha) = -\frac{\exp[w_{\sigma,\alpha,\varepsilon}(z)]}{\{1 + \exp[w_{\sigma,\alpha,\varepsilon}(z)]\}}\frac{z}{(\alpha - z)^2} > 0$$

for $z < 0$, where $w_{\sigma,\alpha,\varepsilon}(z)$ is defined in Eq. (22). □

The method developed in [37] is an efficient approach for solving mathematical programming problems with inequality constraints. It benefits from the nice mathematical properties of exact penalty functions and avoids numerical issues by smoothing these nondifferentiable functions. In Sec. III.B, this method will be adapted to the optimal control framework, and a rigorous convergence proof will be provided. This last one cannot be adapted from that given in [37], and a new demonstration will be given. The resulting approach constitutes a new technique in the optimal control world compared with more classical penalization techniques [28–30] used so far. Indeed, this is the first time that smoothed exact penalty functions are used for dealing with state constraints in optimal control.

B. Smoothed Exact Penalty Approach for Solving State-Constrained Optimal Control Problem $(P)_{\delta_n}$

Adapting the idea given in [37], consider the following two state constraint-free optimal control problems, denoted as $(P^1)_{\alpha,\varepsilon}$ and $(P^2)_{\sigma,\alpha,\varepsilon}$, respectively:

Find

$$\begin{aligned}
\boldsymbol{u}^1_{\alpha,\varepsilon} &= \arg\min_u \\
J^{(1)}_{\alpha,\varepsilon}(\boldsymbol{u}) &= -m(v_f) - \delta_n \int_{v_0}^{v_f} F[v, \boldsymbol{u}(v)]\,\mathrm{d}v \\
&\quad + \int_{v_0}^{v_f} \varphi_{\alpha,\varepsilon}\{g[v, \boldsymbol{x}(v)]\}\,\mathrm{d}v
\end{aligned} \tag{23}$$

such that

$$\begin{aligned}
\dot{\boldsymbol{x}}(v) &= \boldsymbol{A}(v)\boldsymbol{x}(v) + \boldsymbol{B}(v)\frac{\boldsymbol{u}(v)}{m(v)} \\
\dot{m}(v) &= -c(v)\|\boldsymbol{u}(v)\| \\
\|\boldsymbol{u}(v)\| &\leq 1, \qquad v \in [v_0, v_f] \\
\boldsymbol{x}(v_0) &= \boldsymbol{x}_0, \qquad h[\boldsymbol{x}(v_f)] = \boldsymbol{0} \\
m(v_0) &= m_0
\end{aligned}$$

Find

$$\begin{aligned}
\boldsymbol{u}^2_{\sigma,\alpha,\varepsilon} &= \arg\min_u \\
J^{(2)}_{\sigma,\alpha,\varepsilon}(\boldsymbol{u}) &= -m(v_f) - \delta_n \int_{v_0}^{v_f} F[v, \boldsymbol{u}(v)]\,\mathrm{d}v \\
&\quad + \int_{v_0}^{v_f} \psi_{\sigma,\alpha,\varepsilon}\{g[v, \boldsymbol{x}(v)]\}\,\mathrm{d}v
\end{aligned} \tag{24}$$

such that

$$\begin{aligned}
\dot{\boldsymbol{x}}(v) &= \boldsymbol{A}(v)\boldsymbol{x}(v) + \boldsymbol{B}(v)\frac{\boldsymbol{u}(v)}{m(v)} \\
\dot{m}(v) &= -c(v)\|\boldsymbol{u}(v)\| \\
\|\boldsymbol{u}(v)\| &\leq 1, \qquad v \in [v_0, v_f] \\
\boldsymbol{x}(v_0) &= \boldsymbol{x}_0, \qquad h[\boldsymbol{x}(v_f)] = \boldsymbol{0} \\
m(v_0) &= m_0
\end{aligned}$$

where $\alpha > 0$, $\sigma > 0$, and $\varepsilon > 0$ are given values. Function $F(\cdots,\cdots)$ is given in Eq. (8), and δ_n is the same parameter that appears in the performance index of Eq. (18).

An algorithm for solving Eq. (18) is going to be developed now. In this algorithm, a succession of problems $(P^2)_{\sigma,\alpha,\varepsilon}$ associated with decreasing values of σ, α, and ε will be solved. The optimal states associated with the control $\boldsymbol{u}^2_{\sigma,\alpha,\varepsilon}$ will be denoted by $\boldsymbol{x}^2_{\sigma,\alpha,\varepsilon}$ and $m^2_{\sigma,\alpha,\varepsilon}$. In the same way, $\boldsymbol{x}^1_{\alpha,\varepsilon}$ and $m^1_{\alpha,\varepsilon}$ will denote the states associated with the control $\boldsymbol{u}^1_{\alpha,\varepsilon}$. Note that problem $(P^1)_{\alpha,\varepsilon}$ will never have to be solved in the following. Moreover, its solution could not be obtained through the PMP due to the nondifferentiability of function $\varphi_{\alpha,\varepsilon}(.)$. In fact, problem $(P^1)_{\alpha,\varepsilon}$ is introduced only for the needs of the convergence theorem (see Sec. III.C).

Note that the same logarithmic barrier term as in Eq. (18) appears in the performance index of Eq. (24) in order to yield a smooth control law $\boldsymbol{u}^2_{\sigma,\alpha,\varepsilon}(.)$. This last one depends on its associated states $\boldsymbol{x}^2_{\sigma,\alpha,\varepsilon}$, $m^2_{\sigma,\alpha,\varepsilon}$, and costates (denoted again for convenience by $\boldsymbol{p}_x$ and p_m) through Eqs. (9–11) with $\delta = \delta_n$, where $\boldsymbol{u}^0_\delta(v)$ and $\beta^0_\delta(v)$ are replaced, respectively, by $\boldsymbol{u}^2_{\sigma,\alpha,\varepsilon}(v)$ and a new term denoted as $\beta^2_{\sigma,\alpha,\varepsilon}(v)$.

Then, $\boldsymbol{u}^2_{\sigma,\alpha,\varepsilon}(.)$ satisfies the following condition, equivalent to Eq. (12) and (19):

$$\|\boldsymbol{u}^2_{\sigma,\alpha,\varepsilon}(v)\| \in (0,1); \qquad v \in [v_0, v_f] \tag{25}$$

and the following holds:

$$F[v, \boldsymbol{u}^2_{\sigma,\alpha,\varepsilon}(v)] < 0; \qquad v \in [v_0, v_f] \tag{26}$$

The transversality conditions for Eq. (24) are still given by Eq. (17). Moreover, as Eq. (24) has no state constraint, its costate equations can be written in a simple way as follows:

$$\begin{cases} \dot{\boldsymbol{p}}_x(v) = -\boldsymbol{A}(v)^T \boldsymbol{p}_x(v) - \psi'_{\sigma,\alpha,\varepsilon}\{g[v,\boldsymbol{x}(v)]\}\nabla_x g[v,\boldsymbol{x}(v)] \\ \dot{p}_m(v) = -\beta^2_{\sigma,\alpha,\varepsilon}(v)\frac{\|\boldsymbol{B}(v)^T\boldsymbol{p}_x(v)\|}{m^2(v)} \end{cases} \tag{27}$$

where $\psi'_{\sigma,\alpha,\varepsilon}(.)$ denotes the derivative of the function in Eq. (21) given by

$$\forall\ z \in (-\infty, \alpha);$$
$$\psi'_{\sigma,\alpha,\varepsilon}(z) = \frac{\exp[w_{\sigma,\alpha,\varepsilon}(z)]}{1+\exp[w_{\sigma,\alpha,\varepsilon}(z)]}\left(\frac{1}{\varepsilon} + \frac{\alpha}{(\alpha - z)^2}\right) \tag{28}$$

and where $w_{\sigma,\alpha,\varepsilon}(z)$ is defined in Eq. (22). Finally, the components of $\nabla_x g[v, \boldsymbol{x}(v)]$ can be easily computed from Eq. (6), leading to

$$\begin{cases} \frac{\partial g}{\partial x_i}[v,\boldsymbol{x}(v)] = -\frac{x_i(v)}{d_{\min}[1+e\cos(v)]\sqrt{x_1^2(v)+x_2^2(v)+x_3^2(v)}} & (i=1,\dots,3) \\ \frac{\partial g}{\partial x_i}[v,\boldsymbol{x}(v)] = 0 & (i=4,\dots,6) \end{cases} \tag{29}$$
$$v \in [v_0, v_f]$$

Assume first that an initial value $\alpha_0 > 0$ of α is chosen such that the solution of the smoothed unconstrained problem $(P^0)_{\delta_n}$ satisfies the following inequality:

$$g[v, \boldsymbol{x}^0_{\delta_n}(v)] < \alpha_0; \qquad v \in [v_0, v_f] \tag{30}$$

Consider now the following algorithm for solving Eq. (18):

Let $0 < q_1 < q_2 < 1$ with $q_2 < 2q_1$, let $0 < \alpha_{\lim} < \alpha_0$, $\varepsilon_0 > 0$, $\sigma_0 > \alpha^{q_1}_{\lim}$, $0 < \theta < 1$, and $0 < \tau < 1$

Let $k = 0$, end = false

WHILE (end = false)

Solve problem $(P^2)_{\sigma_k,\alpha_k,\varepsilon_k} \to \left(\boldsymbol{x}^2_{\sigma_k,\alpha_k,\varepsilon_k}, m^2_{\sigma_k,\alpha_k,\varepsilon_k}, \boldsymbol{u}^2_{\sigma_k,\alpha_k,\varepsilon_k}\right)$

IF ($\alpha_k \le \alpha_{\lim}$), THEN

end = true

$(\bar{\boldsymbol{x}}_{\delta_n}, \bar{m}_{\delta_n}, \bar{\boldsymbol{u}}_{\delta_n}) \leftarrow (\boldsymbol{x}^2_{\sigma_k,\alpha_k,\varepsilon_k}, m^2_{\sigma_k,\alpha_k,\varepsilon_k}, \boldsymbol{u}^2_{\sigma_k,\alpha_k,\varepsilon_k})$

ELSE

IF $\min\left\{\varepsilon_k, \int_{v_0}^{v_f} \max\{0, g[v, \boldsymbol{x}^2_{\sigma_k,\alpha_k,\varepsilon_k}(v)]\}\,\mathrm{d}v\right\} > \frac{\alpha_k^{q_2}}{\sigma_k}$ THEN

$$\varepsilon_{k+1} = \tau\frac{\alpha_k^{q_2}}{\sigma_k}$$

ELSE

$$\varepsilon_{k+1} = \varepsilon_k$$

END IF

$\alpha_{k+1} = \theta\alpha_k$

$\sigma_{k+1} = \min\{\sigma_k, \alpha^{q_1}_{k+1}\}$

$k = k + 1$

END IF

END WHILE

The sequence $(\alpha_k)_k$ generated by the algorithm is strictly decreasing due to the update rule $\alpha_{k+1} = \theta\alpha_k$ with $\theta \in (0,1)$. In addition, as $\sigma_0 > \alpha^{q_1}_{\lim}$, the following holds:

$$\exists k_1 \ge 0; \quad \forall\ k \ge k_1; \qquad \sigma_{k+1} = \min\{\sigma_k, \alpha^{q_1}_{k+1}\} = \alpha^{q_1}_{k+1} \tag{31}$$

and so the sequence $(\sigma_k)_{k \ge k_1}$ is also strictly decreasing as $q_1 > 0$.

This algorithm is a natural transposition of that given in [37]. Note that problem $(P^2)_{\sigma_k,\alpha_k,\varepsilon_k}$ at iteration k of the preceding algorithm is solved by means of shooting methods, using the solution of $(P^2)_{\sigma_{k-1},\alpha_{k-1},\varepsilon_{k-1}}$ as an initial guess. As δ_n is small, the optimal control $\boldsymbol{u}^2_{\sigma_k,\alpha_k,\varepsilon_k}(.)$ for $k \ge 0$ is smooth but close to a bang-off-bang function [44]. Consequently, the convergence radius of the shooting method is small when solving $(P^2)_{\sigma_k,\alpha_k,\varepsilon_k}$. Thereby, the parameters of the algorithm must be carefully chosen to ensure that the solution of $(P^2)_{\sigma_{k-1},\alpha_{k-1},\varepsilon_{k-1}}$ is sufficiently close to that of $(P^2)_{\sigma_k,\alpha_k,\varepsilon_k}$ (see Sec. IV for more details).

For the same reason (small convergence radius), problem $(P^2)_{\sigma_0,\alpha_0,\varepsilon_0}$ must be solved by a continuation procedure. More precisely, for a given value of $\lambda \in [0,1]$, consider problem $(Q)_\lambda$ defined hereafter.

Find

$$\begin{aligned} w_\lambda &= \arg\min_u \\ K_\lambda(\boldsymbol{u}) &= -m(v_f) - \delta_n \int_{v_0}^{v_f} F[v, \boldsymbol{u}(v)]\,\mathrm{d}v \\ &\quad + \lambda \int_{v_0}^{v_f} \psi_{\sigma_0,\alpha_0,\varepsilon_0}\{g[v, \boldsymbol{x}(v)]\}\,\mathrm{d}v \end{aligned} \tag{32}$$

such that

$$\begin{aligned} &\dot{\boldsymbol{x}}(v) = \boldsymbol{A}(v)\boldsymbol{x}(v) + \boldsymbol{B}(v)\frac{\boldsymbol{u}(v)}{m(v)} \\ &\dot{m}(v) = -c(v)\|\boldsymbol{u}(v)\| \\ &\|\boldsymbol{u}(v)\| \le 1, \qquad v \in [v_0, v_f] \\ &\boldsymbol{x}(v_0) = \boldsymbol{x}_0, \qquad h[\boldsymbol{x}(v_f)] = \boldsymbol{0} \\ &m(v_0) = m_0 \end{aligned}$$

One can remark that $(Q)_0$ is simply problem $(P^0)_{\delta_n}$, and that $(Q)_1$ is problem $(P^2)_{\sigma_0,\alpha_0,\varepsilon_0}$.

Then, using the solution of $(P^0)_{\delta_n}$ as an initial guess, a sequence of problems $(Q)_{\lambda_j}$ $(j = 1, \dots, N)$ is solved for an increasing sequence of values $(0 < \lambda_1 < \cdots < \lambda_N = 1)$, where $N > 0$ is given. For $j \ge 2$, the solution obtained at step $(j-1)$ is used as an initial guess for step j. Thereby, a solution path is built connecting $(P^0)_{\delta_n}$ and $(P^2)_{\sigma_0,\alpha_0,\varepsilon_0}$.

C. Convergence Results

The convergence of the algorithm previously defined cannot be established by directly using the elements given in [37]. The Theorem given hereafter is at the heart of the convergence proof in the optimal control context.

Theorem: Under the following two assumptions of 1) for all $k \ge 0$, problem $(P^2)_{\sigma_k,\alpha_k,\varepsilon_k}$ has a solution satisfying

$$g[v, \boldsymbol{x}^2_{\sigma_k,\alpha_k,\varepsilon_k}(v)] < \alpha_k; \qquad v \in [v_0, v_f]$$

and 2) an index $k_0 \ge 0$ exists such that, for $k \ge k_0$, the solution of $(P^2)_{\sigma_k,\alpha_k,\varepsilon_k}$ satisfies Eq. (6); that is,

$$g[v, \boldsymbol{x}^2_{\sigma_k,\alpha_k,\varepsilon_k}(v)] \le 0; \qquad v \in [v_0, v_f]$$

the following results hold:

1) For all $k \ge k_0$, $\varepsilon_k = \varepsilon_{k_0}$.

2) The sequence $\{J^{(2)}_{\sigma_k,\alpha_k,\varepsilon_{k_0}}(\boldsymbol{u}^2_{\sigma_k,\alpha_k,\varepsilon_{k_0}})\}_{k \ge \max\{k_0,k_1\}}$ [where k_1 is defined in Eq. (31)] is strictly decreasing and converges toward $J_{\delta_n}(\bar{\boldsymbol{u}}_{\delta_n})$ as $k \to \infty$.

3) The sequences $\{J^{(1)}_{\alpha_k,\varepsilon_{k_0}}(\boldsymbol{u}^2_{\sigma_k,\alpha_k,\varepsilon_{k_0}})\}_{k\geq\max\{k_0,k_1\}}$ and $\{J^{(1)}_{\alpha_k,\varepsilon_{k_0}}(\boldsymbol{u}^1_{\alpha_k,\varepsilon_{k_0}})\}_{k\geq\max\{k_0,k_1\}}$ both converge toward $J_{\delta_n}(\bar{\boldsymbol{u}}_{\delta_n})$ as $k\to\infty$.

4) The sequence $\{\boldsymbol{u}^2_{\sigma_k,\alpha_k,\varepsilon_{k_0}}\}_{k\geq\max\{k_0,k_1\}}$ admits a subsequence denoted $\{\boldsymbol{u}^2_{\sigma_{k_j},\alpha_{k_j},\varepsilon_{k_0}}\}_j$ converging toward $\bar{\boldsymbol{u}}_{\delta_n}$ according to the weak-star topology [45] on $L^\infty([v_0,v_f],\Re^3)$ as $j\to\infty$.

5) The sequence $\{\boldsymbol{x}^2_{\sigma_{k_j},\alpha_{k_j},\varepsilon_{k_0}}\}_j$ converges toward $\bar{\boldsymbol{x}}_{\delta_n}$ uniformly on $[v_0,v_f]$ as $j\to\infty$.

6) The sequence $\{m^2_{\sigma_{k_j},\alpha_{k_j},\varepsilon_{k_0}}\}_j$ converges toward $\bar{m}_{\delta_n}$ uniformly on $[v_0,v_f]$ as $j\to\infty$.

Proof: See the Appendix. □

Remember that $L^\infty([v_0,v_f],\Re^3)$ [45] denotes the set of Lebesgue-measurable functions $\boldsymbol{u}$: $[v_0,v_f]\to\Re^3$, such that

$$\|\boldsymbol{u}\|_{L^\infty([v_0,v_f],\Re^3)}=\text{ess sup}\,\|\boldsymbol{u}\|=\inf\{M\in\Re,\mu_L\{v\in[v_0,v_f],\|\boldsymbol{u}(v)\|>M\}=0\}<+\infty$$

where ess sup denotes the essential supremum and $\mu_L(.)$ designates the Lebesgue measure.

Finally, note that assumptions 1 and 2 make no use of the optimal control problem statement. In addition, the convergence proof given in the Appendix makes little use of this statement. The dynamical equations (2–4) need to simply be invertible with respect to the control variable, and the cost function of problem (P) must be bounded below. This means that the approach developed in Sec. III is applicable to a large class of optimal control problems.

IV. Numerical Results

A. Numerical Data

Consider a rendezvous in HEO arising from the SIMBOL-X project [46].

The data are given hereafter as

$$\begin{cases} a=106246.9753\times10^3\ \text{m} & \mu=39860043.6\times10^7\ \text{m}^3\,\text{s}^{-2}\\ e=0.798788 & F_{\max}=0.1\ \text{N}\\ v_0=3.317940017547\ \text{rad} & I_{\text{sp}}=220.0\ \text{s}\\ v_f=3.349161118514\ \text{rad} & m_0=960.0\ \text{kg}\end{cases}\tag{33}$$

$$\begin{cases} X(t_0)=\tilde{X}(v_0)=-100.0\ \text{m} & \frac{\mathrm{d}X}{\mathrm{d}t}(t_0)=0.0\ \text{m}\,\text{s}^{-1}\\ Y(t_0)=\tilde{Y}(v_0)=-100.0\ \text{m} & \frac{\mathrm{d}Y}{\mathrm{d}t}(t_0)=0.0\ \text{m}\,\text{s}^{-1}\\ Z(t_0)=\tilde{Z}(v_0)=-100.0\ \text{m} & \frac{\mathrm{d}Z}{\mathrm{d}t}(t_0)=0.0\ \text{m}\,\text{s}^{-1}\end{cases}\tag{34}$$

$$\begin{cases} X(t_f)=\tilde{X}(v_f)=500.0\ \text{m} & \frac{\mathrm{d}X}{\mathrm{d}t}(t_f)=0.0\ \text{m}\,\text{s}^{-1}\\ Y(t_f)=\tilde{Y}(v_f)=500.0\ \text{m} & \frac{\mathrm{d}Y}{\mathrm{d}t}(t_f)=0.0\ \text{m}\,\text{s}^{-1}\\ Z(t_f)=\tilde{Z}(v_f)=500.0\ \text{m} & \frac{\mathrm{d}Z}{\mathrm{d}t}(t_f)=0.0\ \text{m}\,\text{s}^{-1}\end{cases}\tag{35}$$

The initial date t_0 is fixed to $t_0=0.0$ s. The final date t_f corresponding to the true anomaly v_f can be easily computed using Kepler's equation, leading here to $t_f=8000.0$ s. The initial and terminal conditions in Eqs. (34) and (35) are given in terms of the original coordinates of the chaser and in terms of their derivatives with respect to time. Thus, they have to be transformed in order to yield the corresponding vectors $\boldsymbol{x}_0$ and $\boldsymbol{x}_f$. Indeed, function $h(.)$ takes the form $h[\boldsymbol{x}(v_f)]=\boldsymbol{x}(v_f)-\boldsymbol{x}_f$.

For the sake of simplicity, in all the figures presented in Secs. IV.B and IV.C, the original coordinates of the chaser will be denoted by X, Y, and Z, and $\boldsymbol{u}$ will denote the control vector, whatever the problem under consideration.

B. Solving the Unconstrained Problem

Using the technique developed in [44], problem (P^0) is solved. Remember that the solution of this last one is approximated by that of $(P^0)_{\delta_n}$ (see Sec. II.C), where δ_n has been fixed here to $\delta_n=9.8785\times10^{-9}$. The fuel consumption and the minimum distance between the two satellites are given hereafter as

$$m_0-m^0_{\delta_n}(v_f)=0.1433\ \text{kg}$$

$$\min_{v\in[v_0,v_f]}d_{\min}\{1-g[v,\boldsymbol{x}^0_{\delta_n}(v)]\}=2.9103\ \text{m}$$

The time histories of the original coordinates of the chaser and those of their time derivatives are presented in Figs. 1 and 2. Figures 3 and 4 show the time variations of the norm of the control and those of its components.

Notice that, due to the very small value chosen for δ_n, the control appears to be bang-off-bang on Fig. 3. In addition, Fig. 3 indicates that the control law is made of two thrust arcs located at the beginning and at the end of the rendezvous.

In Fig. 4, the bold lines correspond to the thrust arcs. During coast arcs, the components of the normalized thrust vector (in thin line) are not significant. Finally, Fig. 5 shows the variations of the distance between the satellites with respect to time. One can remark that the distance takes its minimum value at around $t=1800.0$ s.

C. Solving the State-Constrained Problem

1. *Introduction*

The problem defined in Eq. (18) is going to be solved now by using the algorithm developed in Sec. III.

The first issue consists of choosing the parameters of the algorithm. Unfortunately, there is no explicit rule in [37] for

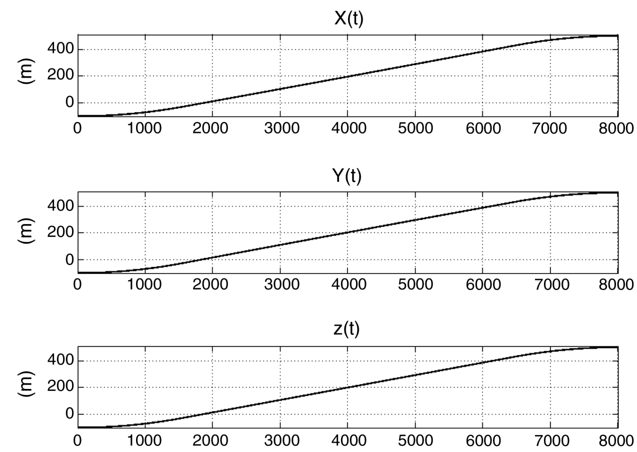

Fig. 1 Unconstrained problem: relative position vector in the local orbital frame.

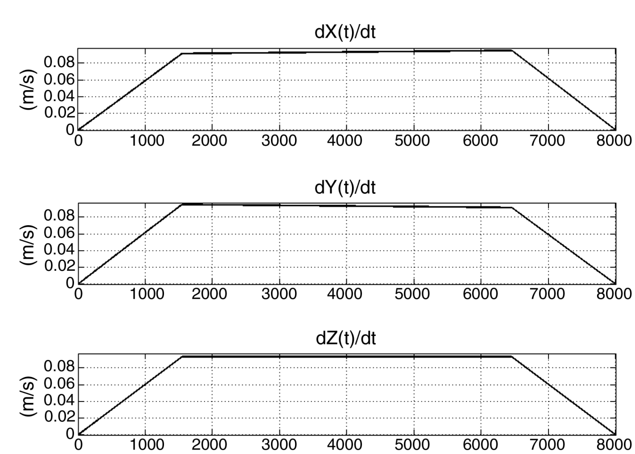

Fig. 2 Unconstrained problem: relative velocity vector with respect to time in the local orbital frame.

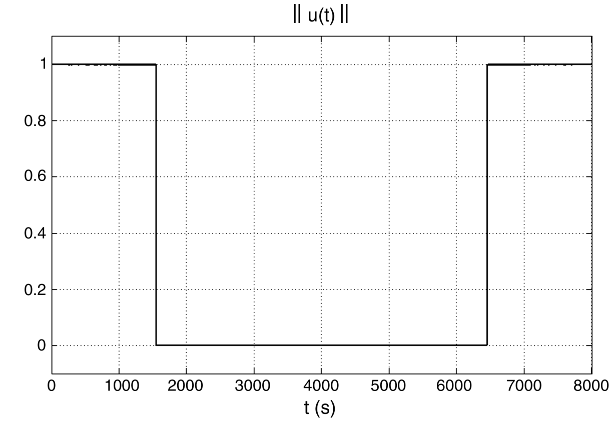

Fig. 3 Unconstrained problem: norm of the normalized thrust vector *u*.

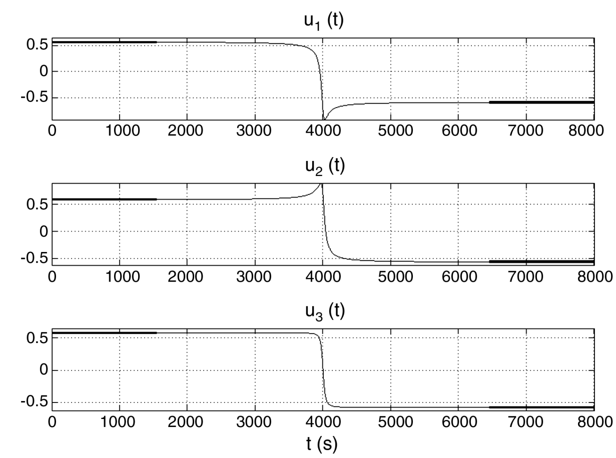

Fig. 4 Unconstrained problem: components of the normalized thrust vector *u*.

determining these parameters. Moreover, the convergence Theorem in Sec. III indicates that under assumptions 1 and 2, the convergence of the algorithm is guaranteed, whatever the values of these parameters, provided that

$$0 < q_1 < q_2 < 1; \qquad q_2 < 2q_1; \qquad 0 < \alpha_{\lim} < \alpha_0; \qquad \varepsilon_0 > 0$$
$$\sigma_0 > \alpha_{\lim}^{q_1}; \qquad 0 < \theta < 1; \qquad 0 < \tau < 1$$

and that Eq. (30) is satisfied.

Then, in the test cases presented in Secs. IV.C.2 and IV.C.3, parameters α_0 and σ_0 are empirically set to $\alpha_0 = 0.98$ and $\sigma_0 = 1.0$. For each test case, the value of $\alpha_{\lim}$ is chosen as follows. At a given index $k_{\lim}$ of the algorithm (which depends on the test case), numerical issues arise when solving problem $(P^2)_{\sigma_{k\lim},\alpha_{k_{\lim}},\varepsilon_{k_{\lim}}}$, because $\alpha_{k_{\lim}}$ and $\sigma_{k_{\lim}}$ are too small and the problem becomes ill-conditioned [function $\psi_{\sigma_{k\lim},\alpha_{k_{\lim}},\varepsilon_{k_{\lim}}}(.)$ defined in Eq. (21) is too close to the nondifferentiable function $\varphi_{\alpha_{k_{\lim}},\varepsilon_{k_{\lim}}}(.)$ defined in Eq. (20)]. Then, parameter $\alpha_{\lim}$ is simply set to $\alpha_{\lim} = \alpha_{k_{\lim}-1}$. As far as parameter ε_0 is concerned, it is first set to the following value of $\varepsilon_0 = 0.1$. Then, ε_0 is reduced until problems $(Q)_{\lambda_j}(j = 1, \ldots, N)$, defined in Eq. (32), are successfully solved, the sequence $(\lambda_j)_j(j = 1, \ldots, N)$ and N being fixed. Parameters q_1, q_2, θ, and τ directly influence the convergence speed. But remember that at each step k of the algorithm, the solution of $(P^2)_{\sigma_{k-1},\alpha_{k-1},\varepsilon_{k-1}}$ must be sufficiently close to that of $(P^2)_{\sigma_k,\alpha_k,\varepsilon_k}$ in order to make the shooting method converge when solving this last problem. This means, in particular, that θ and τ must be sufficiently close to one in order to yield slowly decreasing sequences $(\sigma_k)_k$, $(\alpha_k)_k$, and $(\varepsilon_k)_k$. This is why they are set to $\theta = 0.99$ and $\tau = 0.9$ in all the numerical experimentations. For the same reason, parameters q_1 and q_2 must be sufficiently small. They are first set to $q_1 = 0.3$ and $q_2 = 0.5$ and then reduced each time the shooting method encounters difficulties when solving problem $(P^2)_{\sigma_k,\alpha_k,\varepsilon_k}$ at a given index k of the algorithm.

Note that all these rules are purely empirical. Their aim is to ensure the robustness of the algorithm at the expense of convergence speed.

2. *First Test Case*

The safety minimum distance is fixed to $d_{\min} = 50.0$ m. The parameters of the algorithm are chosen according to the rules given in Sec. IV.C.1, leading here to the following values:

$$q_1 = 0.3; \qquad q_2 = 0.5; \qquad \alpha_{\lim} = 4.73 \times 10^{-4}; \qquad \alpha_0 = 0.98$$
$$\varepsilon_0 = 0.0998; \qquad \sigma_0 = 1.0; \qquad \theta = 0.99; \qquad \tau = 0.9$$

The number of iterations performed by the algorithm are equal to $k_{\lim} - 1 = 918$ (see Sec. IV.C.1).

The fuel expenditure and the minimum distance between the two satellites obtained at the convergence are given hereafter as

$$m_0 - \bar{m}_{\delta_n}(v_f) = 0.1585 \text{ kg}$$
$$\min_{v\in[v_0,v_f]} d_{\min}\{1 - g[v, \bar{\boldsymbol{x}}_{\delta_n}(v)]\} = 50.0444 \text{ m}$$

As expected, the fuel consumption is greater than that obtained for the unconstrained problem.

Figure 6 shows the variations of the fuel consumption as a function of the iteration index k of the algorithm. The fuel consumption obtained at step k is given by $\Delta m_k = m_0 - m^2_{\sigma_k,\alpha_k,\varepsilon_k}(v_f)$. One can notice, on Fig. 6, that the fuel expenditure decreases with the value of k.

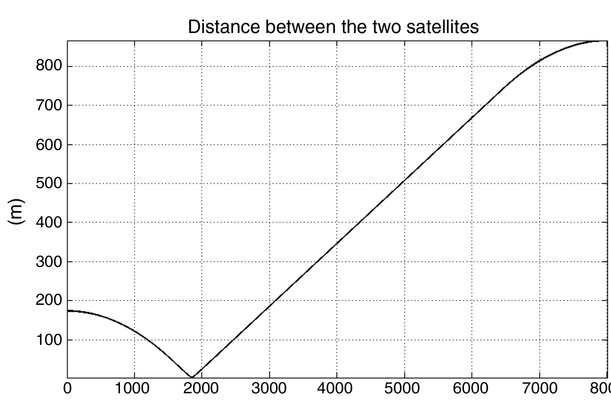

Fig. 5 Unconstrained problem: distance between the chaser satellite and the target satellite.

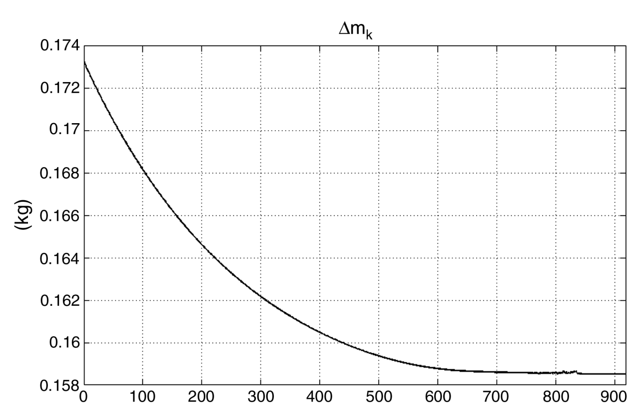

Fig. 6 State-constrained problem: $d_{\min} = 50$ m: fuel consumption during the course of the algorithm.

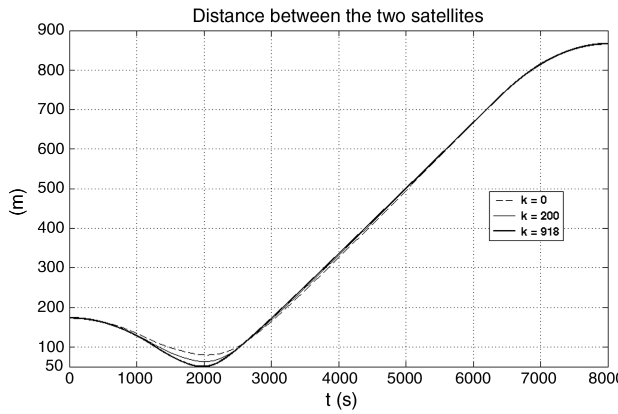

Fig. 7 State-constrained problem, $d_{\min} = 50$ m: distance between the satellites for different values of k.

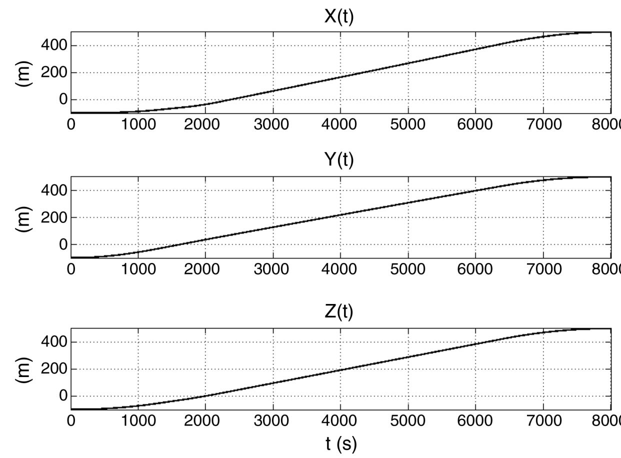

Fig. 9 State-constrained problem, $d_{\min} = 50$ m: relative position vector in the local orbital frame.

The time history of the distance between the satellites is presented in Fig. 7. Different plots corresponding to intermediate solutions obtained during the course of the algorithm are provided. These correspond to the following values of the iteration index: $k = 0$, $k = 200$, and $k = 918$ (final solution).

It is clear from Fig. 7 that the state constraint in Eq. (6) is strictly satisfied at each step $k \geq 0$ of the algorithm. Therefore, assumptions 1 and 2 of the convergence Theorem are satisfied, and the following holds $\forall\ k \geq 0$, $\varepsilon_k = \varepsilon_0$.

The variations of the distance between the satellites in Fig. 7 for $k = 918$ do not allow us to determine if Eq. (6) is active on a small interval in true anomaly for Eq. (18) [and thus for Eq. (5)] or if there is only a contact point. This difficulty comes directly from the fact that the state constraint in Eq. (6) is strictly satisfied at every step of the algorithm. Even if the solution obtained is an accurate approximation of that of Eq. (18) (due to the small value of $\alpha_{\lim}$), the structure of the optimal trajectory could be determined with certainty only for smaller values of $\alpha_{\lim}$. Unfortunately, convergence issues arise when $\alpha_{\lim} < 4.73 \times 10^{-4}$ (see the rules given in Sec. IV.C.1 for determining the parameters of the algorithm).

The time history of the control norm is presented in Fig. 8 below. Different plots corresponding to intermediate solutions obtained during the course of the algorithm are provided. The last ones correspond, again, to the following values of the iteration index: $k = 0$, $k = 200$, and $k = 918$ (final solution). Thus, Fig. 8 illustrates the convergence of the sequence $\{\|\boldsymbol{u}^2_{\sigma_k,\alpha_k,\varepsilon_{k_0}}\|\}_k$. In addition, one can notice that by comparing Figs. 3 and 8, a third thrust arc appears on Fig. 8 in order to deal with the state constraint.

Figures 9 and 10 show the time variations of the original coordinates of the chaser and those of their derivatives with respect to time. They correspond to the solution obtained at the convergence of the algorithm ($k = 918$). In the same way, the time histories of the control components are presented in Fig. 11.

3. Second Test Case

Consider now the case where $d_{\min} = 140.0$ m. The parameters of the algorithm are chosen, again according to the rules given in Sec. IV.C.1, leading to the following values:

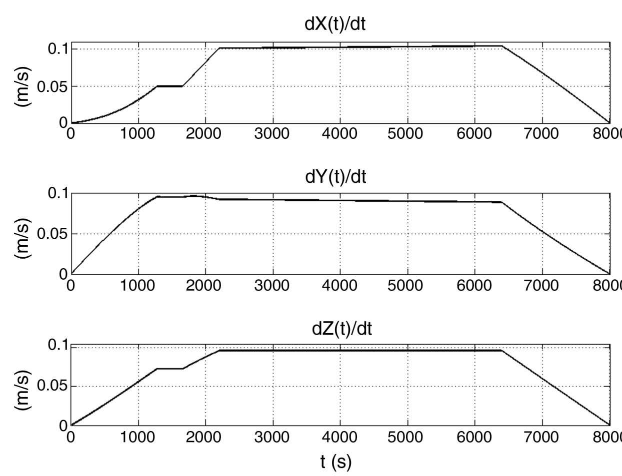

Fig. 10 State-constrained problem, $d_{\min} = 50$ m: relative velocity vector with respect to time in the local orbital frame.

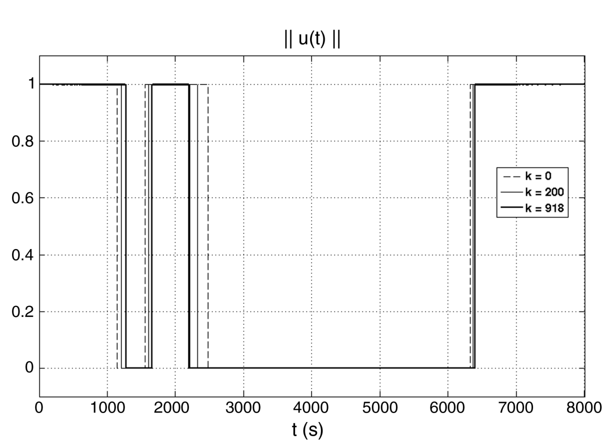

Fig. 8 State-constrained problem, $d_{\min} = 50$ m: norm of the thrust vector u for different values of k.

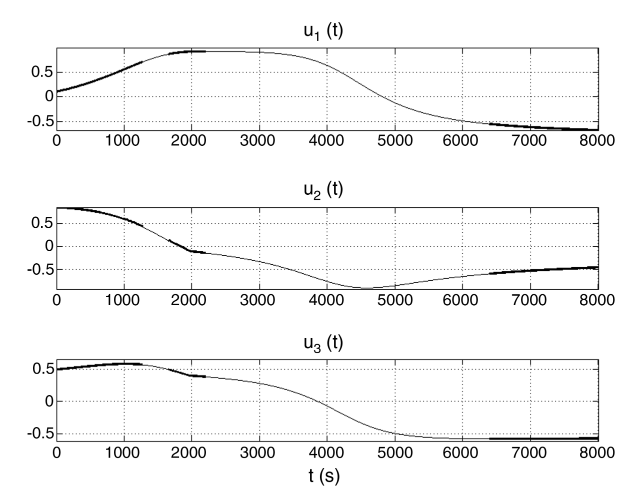

Fig. 11 State-constrained problem, $d_{\min} = 50$ m: components of the normalized thrust vector u.

$$q_1 = 0.3; \qquad q_2 = 0.5; \qquad \alpha_{\lim} = 2.19 \times 10^{-4}; \qquad \alpha_0 = 0.98$$
$$\varepsilon_0 = 6.09 \times 10^{-4}; \qquad \sigma_0 = 1.0; \qquad \theta = 0.99; \qquad \tau = 0.9$$

The number of iterations performed by the algorithm is equal here to $k_{\lim} - 1 = 963$ (see Sec. IV.C.1).

Solving Eq. (18) by means of the algorithm developed in Sec. III leads to the following results:

$$m_0 - \bar{m}_{\delta_n}(v_f) = 0.2175 \text{ kg}$$
$$\min_{v \in [v_0, v_f]} d_{\min}\{1 - g[v, \bar{\boldsymbol{x}}_{\delta_n}(v)]\} = 140.0200 \text{ m}$$

The fuel consumption is greater than that obtained in Sec. IV.C.2. This is due to the greater value of $d_{\min}$ used in this second test case.

Figure 12 shows the variations of the control norm with respect to time. The thrust arcs appear to be longer than those given in Fig. 8. This is due again to the value of $d_{\min}$, which is greater than that used in Sec. IV.C.2. Finally, the time history of the distance between the satellites is presented in Fig. 13.

Because of the small value of ε_0, the control variable and the distance between the satellites, considered as functions of time, vary very weakly with the iteration index k of the algorithm. For this reason, plots corresponding to different values of k are not provided in Figs. 12 and 13. It would be impossible to distinguish between them. As in Sec. IV.C.2, the state constraint in Eq. (6) is strictly satisfied at each step $k \geq 0$. Thus, assumptions 1 and 2 are satisfied, and the following holds $\forall\ k \geq 0$, $\varepsilon_k = \varepsilon_0$.

Figure 13 shows that the distance between the satellites remains very close to $d_{\min}$ during an interval centered on $t = 2000.0$ s. In addition, as assumptions 1 and 2 are satisfied, the convergence Theorem certifies that the solution obtained at the convergence of the algorithm is close to that of Eq. (18). Thus, Eq. (6) is certainly active on a nonzero interval in true anomaly for Eqs. (18) and (5). Indeed, according to the PMP [21,22], the state constraint can be satisfied as an equality on a given interval by the solutions of these two state-constrained problems.

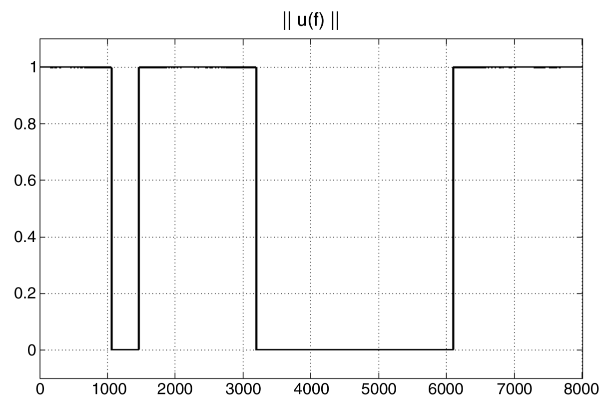

Fig. 12 State-constrained problem, $d_{\min} = 140$ m: norm of the normalized thrust vector u.

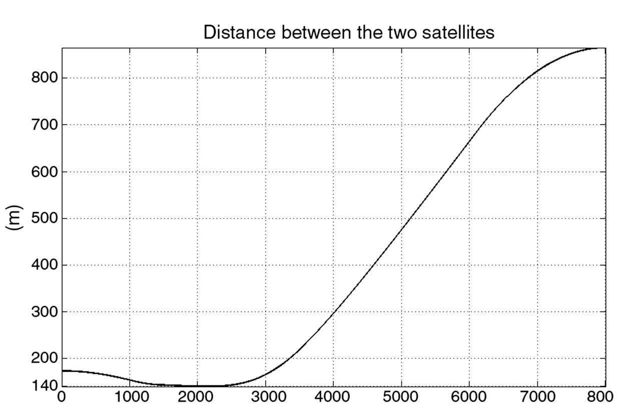

Fig. 13 State-constrained problem, $d_{\min} = 140$ m: distance between the chaser satellite and the target satellite.

V. Conclusions

An efficient numerical method for computing constrained fuel-optimal continuous-thrust rendezvous trajectories is designed in this paper. By adapting the idea of using smoothed exact penalty functions to the optimal control context, it is shown that it is possible to solve this kind of state-constrained problem through PMP by simply solving a sequence of unconstrained problems.

A convergence proof is given, and the method is successfully applied to a rendezvous on HEOs. The method needs to be further validated in different rendezvous problems, for example, by considering low Earth orbit applications where orbital perturbations such as the J_2 term of the Earth's potential are introduced in the dynamical equations.

Finally, as the methodology developed is this paper is a generic approach to deal with inequality state constraints in optimal control, it can also applied to different problems in which state constraints are critical. The optimization of reentry trajectories under the thermal flux constraint or the optimization of interplanetary trajectories with minimum flyby altitude constraint are typical instances of such problems.

Appendix: Proof of the Convergence Theorem

The first point of the Theorem is straightforward and relies directly on assumption 2 and on the update rule of ε_k in the algorithm.

By using the definition of Eq. (24), together with Lemma 2, Lemma 3, assumption 2, and the update rules of σ_k and α_k in the algorithm that lead to $\alpha_{k+1} < \alpha_k$ and $\sigma_{k+1} < \sigma_k$ for $k \geq k_1$ [see Eq. (31)], it appears that for any $k \geq \max\{k_0, k_1\}$,

$$\begin{aligned} J^{(2)}_{\sigma_{k+1},\alpha_{k+1},\varepsilon_{k_0}}(\boldsymbol{u}^2_{\sigma_{k+1},\alpha_{k+1},\varepsilon_{k_0}}) &\leq J^{(2)}_{\sigma_{k+1},\alpha_{k+1},\varepsilon_{k_0}}(\boldsymbol{u}^2_{\sigma_k,\alpha_k,\varepsilon_{k_0}}) \\ &< J^{(2)}_{\sigma_{k+1},\alpha_k,\varepsilon_{k_0}}(\boldsymbol{u}^2_{\sigma_k,\alpha_k,\varepsilon_{k_0}}) < J^{(2)}_{\sigma_k,\alpha_k,\varepsilon_{k_0}}(\boldsymbol{u}^2_{\sigma_k,\alpha_k,\varepsilon_{k_0}}) \end{aligned}$$

Thus, the sequence

$$\{J^{(2)}_{\sigma_k,\alpha_k,\varepsilon_{k_0}}(\boldsymbol{u}^2_{\sigma_k,\alpha_k,\varepsilon_{k_0}})\}_{k \geq \max\{k_0,k_1\}}$$

is strictly decreasing.

Moreover, by using Eq. (26) together with the dynamical equation of $m^2_{\sigma_k,\alpha_k,\varepsilon_{k_0}}(.)$ in Eq. (24) and, as for $k \geq 0$, the following holds: $\psi_{\sigma_k,\alpha_k,\varepsilon_{k_0}}(z) > 0$ for $z \in (-\infty, \alpha_k)$, it is possible to write that, for any $k \geq \max\{k_0, k_1\}$,

$$J^{(2)}_{\sigma_k,\alpha_k,\varepsilon_{k_0}}(\boldsymbol{u}^2_{\sigma_k,\alpha_k,\varepsilon_{k_0}}) > -m^2_{\sigma_k,\alpha_k,\varepsilon_{k_0}}(v_f) \geq -m_0$$

so the preceding sequence is also bounded below. Consequently, it converges toward a limit denoted as $J_{\lim}$ as $k \to \infty$.

Now, using Lemma 1 together with the triangle inequality leads for any $k \geq \max\{k_0, k_1\}$ to

$$\begin{aligned} |J^{(1)}_{\alpha_k,\varepsilon_{k_0}}(\boldsymbol{u}^2_{\sigma_k,\alpha_k,\varepsilon_{k_0}}) - J_{\lim}| &\leq |J^{(1)}_{\alpha_k,\varepsilon_{k_0}}(\boldsymbol{u}^2_{\sigma_k,\alpha_k,\varepsilon_{k_0}}) - J^{(2)}_{\sigma_k,\alpha_k,\varepsilon_{k_0}}(\boldsymbol{u}^2_{\sigma_k,\alpha_k,\varepsilon_{k_0}})| \\ &+ |J^{(2)}_{\sigma_k,\alpha_k,\varepsilon_{k_0}}(\boldsymbol{u}^2_{\sigma_k,\alpha_k,\varepsilon_{k_0}}) - J_{\lim}| < \sigma_k(v_f - v_0)\log(2) \\ &+ |J^{(2)}_{\sigma_k,\alpha_k,\varepsilon_{k_0}}(\boldsymbol{u}^2_{\sigma_k,\alpha_k,\varepsilon_{k_0}}) - J_{\lim}| \end{aligned}$$

Then, as the sequence $(\sigma_k)_{k \geq k_1}$, generated by the algorithm, is strictly decreasing and converges toward zero as $k \to \infty$, it is possible to deduce from the preceding inequality that

$$\{J^{(1)}_{\alpha_k,\varepsilon_{k_0}}(\boldsymbol{u}^2_{\sigma_k,\alpha_k,\varepsilon_{k_0}})\}_{k \geq \max\{k_0,k_1\}} \to J_{\lim}$$

as $k \to \infty$.

On the other hand, by using Lemma 1 again, together with the definition of Eqs. (23) and (24), one can write that for any $k \geq \max\{k_0, k_1\}$,

$$J^{(1)}_{\alpha_k,\varepsilon_{k_0}}\left(\boldsymbol{u}^2_{\sigma_k,\alpha_k,\varepsilon_{k_0}}\right) - \sigma_k(v_f - v_0)\log(2) < J^{(2)}_{\sigma_k,\alpha_k,\varepsilon_{k_0}}\left(\boldsymbol{u}^2_{\sigma_k,\alpha_k,\varepsilon_{k_0}}\right) - \sigma_k(v_f - v_0)\log(2) \leq J^{(2)}_{\sigma_k,\alpha_k,\varepsilon_{k_0}}\left(\boldsymbol{u}^1_{\alpha_k,\varepsilon_{k_0}}\right) - \sigma_k(v_f - v_0)\log(2) < J^{(1)}_{\alpha_k,\varepsilon_{k_0}}\left(\boldsymbol{u}^1_{\alpha_k,\varepsilon_{k_0}}\right) \leq J^{(1)}_{\alpha_k,\varepsilon_{k_0}}\left(\boldsymbol{u}^2_{\sigma_k,\alpha_k,\varepsilon_{k_0}}\right)$$

Thereby, the sequence $\{J^{(1)}_{\alpha_k,\varepsilon_{k_0}}(\boldsymbol{u}^1_{\alpha_k,\varepsilon_{k_0}})\}_{k\geq\max\{k_0,k_1\}}$ being bounded above and below by two sequences converging toward $J_{\lim}$, it converges itself toward $J_{\lim}$ as $k \to \infty$.

Now, using the definition of Eq. (18) together with assumption 2, one can write that for any $k \geq \max\{k_0, k_1\}$,

$$J^{(1)}_{\alpha_k,\varepsilon_{k_0}}\left(\boldsymbol{u}^2_{\sigma_k,\alpha_k,\varepsilon_{k_0}}\right) = J\left(\boldsymbol{u}^2_{\sigma_k,\alpha_k,\varepsilon_{k_0}}\right) - \delta_n \int_{v_0}^{v_f} F[v, \boldsymbol{u}^2_{\sigma_k,\alpha_k,\varepsilon_{k_0}}(v)]\,\mathrm{d}v = J_{\delta_n}\left(\boldsymbol{u}^2_{\sigma_k,\alpha_k,\varepsilon_{k_0}}\right) \geq J_{\delta_n}(\bar{\boldsymbol{u}}_{\delta_n})$$

so that

$$J_{\lim} = \lim_{k\to+\infty} J^{(1)}_{\alpha_k,\varepsilon_{k_0}}\left(\boldsymbol{u}^2_{\sigma_k,\alpha_k,\varepsilon_{k_0}}\right) \geq J_{\delta_n}(\bar{\boldsymbol{u}}_{\delta_n})$$

On the other hand, as for any $k \geq \max\{k_0, k_1\}$,

$$J^{(1)}_{\alpha_k,\varepsilon_{k_0}}\left(\boldsymbol{u}^1_{\alpha_k,\varepsilon_{k_0}}\right) \leq J^{(1)}_{\alpha_k,\varepsilon_{k_0}}(\bar{\boldsymbol{u}}_{\delta_n}) = J_{\delta_n}(\bar{\boldsymbol{u}}_{\delta_n})$$

one also has

$$J_{\lim} = \lim_{k\to+\infty} J^{(1)}_{\alpha_k,\varepsilon_{k_0}}\left(\boldsymbol{u}^1_{\alpha_k,\varepsilon_{k_0}}\right) \leq J_{\delta_n}(\bar{\boldsymbol{u}}_{\delta_n})$$

In conclusion, $J_{\lim} = J_{\delta_n}(\bar{\boldsymbol{u}}_{\delta_n})$ and points 2 and 3 of the Theorem are proved.

Now, follow the same sketch as in the demonstration of Filippov's existence theorem [47]. First, Eq. (2) can be inverted, and the control $\boldsymbol{u}(v)$ can be expressed as a smooth function of v, $\boldsymbol{x}(v)$, $\dot{\boldsymbol{x}}(v)$, and $m(v)$. In addition, from point 2 and assumption 2, it is possible to deduce that $\{\boldsymbol{u}^2_{\sigma_k,\alpha_k,\varepsilon_{k_0}}\}_{k\geq\max\{k_0,k_1\}}$ is a minimizing sequence for Eq. (18). Then, by using theorem 4 from [48] and the lower closure theorem (8.8.i) from [47] (p. 303), it is possible to show that this sequence admits a subsequence denoted as $\{\boldsymbol{u}^2_{\sigma_{k_j},\alpha_{k_j},\varepsilon_{k_0}}\}_j$ converging toward $\bar{\boldsymbol{u}}_{\delta_n}$ for the weak-star topology on $L^\infty([v_0, v_f], \Re^3)$ as $j \to \infty$. In addition, the corresponding sequences $\{\boldsymbol{x}^2_{\sigma_{k_j},\alpha_{k_j},\varepsilon_{k_0}}\}_j$ and $\{m^2_{\sigma_{k_j},\alpha_{k_j},\varepsilon_{k_0}}\}_j$ uniformly converge toward $\bar{\boldsymbol{x}}_{\delta_n}$ and $\bar{m}_{\delta_n}$ on $[v_0, v_f]$.

This concludes the proof by verifying points 4, 5, and 6 of the Theorem. □

Acknowledgment

The greatest thanks to my colleague Jean-Claude Berges from the Centre National d'Etudes Spatiales, involved in the PRISMA project, for fruitful discussions and advice.

References

[1] Sjöberg, F., Karlsson, A., and Jakobsson, B., "PROBA-3: A Formation Flying Demonstration Mission on the Verge to be Realised," *Proceedings of the 3rd International Symposium on Formation Flying, Missions and Technologies* [online], ESA SP 654, Paris, 2008.

[2] Persson, S., Veldman, S., and Bodin, P., "PRISMA-A Formation Flying Project in Implementation Phase," *Acta Astronautica*, Vol. 65, Nos. 9–10, 2009, pp. 1360–1374. doi:10.1016/j.actaastro.2009.03.067

[3] Gogibus, E., Charbonnel, H., and Delpy, P., "Autonomous and Robust Rendezvous Guidance on Elliptical Orbit Subject to J_2 Perturbation," *21st International Symposium on Space Flight Dynamics* [online], Toulouse, France, Sept. 2009, http://www.mediatec-dif.com/issfd/FflyingII/Gogibus.pdf [retrieved 4 Jan. 2010].

[4] Delpech, M., Dubois, J.-B., Riedel, J. E., and Guinn, J. R., "Description of the Rendezvous Experiment Designed for 2007 Mars Premier Mission," *17th International Symposium on Space Flight Dynamics* [online], Moscow, June 2003, http://trs-new.jpl.nasa.gov/dspace/bitstream/2014/7566/1/03-1511.pdf [retrieved 4 January 2010].

[5] Kaiser, C., Sjoberg, F., Delcura, J. M., and Eilertsen, B., "SMART-OLEV: An Orbital Life Extension Vehicle for Servicing Commercial Spacecrafts in GEO," *Acta Astronautica*, Vol. 63, Nos. 1–4, 2008, pp. 400–410. doi:10.1016/j.actaastro.2007.12.053

[6] Tillerson, M., and How, J. P., "Formation Flying Control in Eccentric Orbits," AIAA Guidance, Navigation, and Control Conference, Montreal, Canada, AIAA Paper 2001-4092, 2001.

[7] Lim, H. -C., Bang, H. -C., Park, K. -D., and Lee, W. -K., "Optimal Formation Trajectory-Planning Using Parameter Optimization Technique," *Journal of Astronomy and Space Sciences*, Vol. 21, No. 3, 2004, pp. 209–220. doi:10.5140/JASS.2004.21.3.209

[8] Junge, O., and Ober-Blobaum, S., "Optimal Reconfiguration of Formation Flying Satellites," *44th IEEE Conference on Decision and Control, Inst. of Electrical and Electronics Engineers*, IEEE Publ., Piscataway, NJ, 2005, pp. 66–71.

[9] Yang, G., Yang, Q., Kapila, V., Palmer, D., and Vaidyanathan, R., "Fuel Optimal Maneuvers for Multiple Spacecraft Formation Reconfiguration using Multiagent Optimization," *International Journal of Robust and Nonlinear Control*, Vol. 12, Nos. 2–3, 2002, pp. 243–283. doi:10.1002/rnc.684

[10] Rauwolf, G., and Coverstone-Caroll, V., "Near-optimal Low-thrust Orbit Transfers Generated by a Genetic Algorithm," *Journal of Spacecraft and Rockets*, Vol. 33, No. 6, 1996, pp. 859–862. doi:10.2514/3.26850

[11] Pisarevsky, D., and Gurfil, P., "A Memetic Algorithm for Optimizing High-Inclination Multiple Gravity-Assist Orbits," *Proceedings of the 2009 IEEE Congress on Evolutionary Computation*, Trondheim, Norway, IEEE Publ., Piscataway, NJ, May 2009, pp. 86–93.

[12] Garcia, I., and How, J. P., "Trajectory Optimization for Satellite Reconfiguration Maneuvers with Position and Attitude Constraints," *IEEE American Control Conference*, IEEE Publ., Piscataway, NJ, 2005, pp. 889–895.

[13] Singh, G., and Hadaegh, F., "Autonomous Path-Planning for Formation-Flying Applications," *16th International Symposium on Space Flight Dynamics* [online], Pasadena, CA, 2001, http://trs-new.jpl.nasa.gov/dspace/bitstream/2014/13424/1/01-2358.pdf [retrieved 24 Oct. 2007].

[14] Kim, Y., Mesbahi, M., and Hadaegh, F. Y., "Multiple-Spacecraft Reconfiguration Through Collision Avoidance, Bouncing, and Stalemates," *Journal of Optimization Theory and Applications*, Vol. 122, No. 2, 2004, pp. 323–343. doi:10.1023/B:JOTA.0000042524.57088.8b

[15] Massari, M., and Bernelli-Zazzera, F., "Optimization of Low-Thrust Reconfiguration Maneuvers for Spacecraft Flying in Formation," *Journal of Guidance, Control, and Dynamics*, Vol. 32, No. 5, 2009, pp. 1629–1638. doi:10.2514/1.37335

[16] Wu, B., Wang, D., Poh, E. K., and Xu, G., "Nonlinear Optimization of Low-Thrust Trajectory for Satellite Formation: Legendre Pseudospectral Approach," *Journal of Guidance, Control, and Dynamics*, Vol. 32, No. 4, 2009, pp. 1371–1381. doi:10.2514/1.37675

[17] Richards, A., How, J. P., Schouwenaars, T., and Feron, E., "Plume Avoidance Maneuver Planning Using Mixed Integer Linear Programming," AIAA Guidance, Navigation, and Control Conference, AIAA Paper 2001-4091, 2001.

[18] Richards, A., Schouwenaars, T., How, J. P., and Feron, E., "Spacecraft Trajectory Planning with Avoidance Constraints using Mixed-Integer Linear Programming," *Journal of Guidance, Control, and Dynamics*, Vol. 25, No. 4, 2002, pp. 755–764. doi:10.2514/2.4943

[19] Cetin, B., Bikdash, M., and Hadaegh, F. Y., "Hybrid Mixed-Llogical Linear Programming Algorithm for Collision-Free Optimal Path Planning," *IET Control Theory and Applications*, Vol. 1, No. 2, 2007, pp. 522–531. doi:10.1049/iet-cta:20050432

[20] Louembet, C., Kara-Zaïri, M., Arzelier, D., and Théron, A., "Solving Fuel-Optimal Orbital Homing Problem with Continuous Thrust using Direct Methods," *21st International Symposium on Space Flight Dynamics* [online], Toulouse, France, Sept. 2009, http://www.mediatec-dif.com/issfd/OptimiII/Louembet.pdf [retrieved 4 Jan. 2010].

[21] Pontryagin, L., *Optimal Regulation Processes*, *American Mathematical Society Translations*, Vol. 18, American Mathematical Society,

Providence, RI, 1961, pp. 17–66.

[22] Bryson, A. E., and Ho, Y. C., *Applied Optimal Control*, Hemisphere, New York, 1975, pp. 42–125.

[23] Betts, J. T., "Survey of Numerical Methods for Trajectory Optimization," *Journal of Guidance, Control, and Dynamics*, Vol. 21, No. 2, 1998, pp. 193–207.
doi:10.2514/2.4231

[24] Beard, R. W., McLain, T. W., and Hadaegh, F. Y., "Fuel Optimization for Constrained Rotation of Spacecraft Formations," *Journal of Guidance, Control, and Dynamics*, Vol. 23, No. 2, 2000, pp. 339–346.
doi:10.2514/2.4528

[25] Thevenet, J. -B., and Epenoy, R., "Minimum-Fuel Deployment for Spacecraft Formations via Optimal Control," *Journal of Guidance, Control, and Dynamics*, Vol. 31, No. 1, 2008, pp. 101–113.
doi:10.2514/1.30364

[26] Kim, Y., Mesbahi, M., and Hadaegh, F. Y., "Dual-Spacecraft Formation Flying in Deep Space: Optimal Collision-Free Reconfigurations," *Journal of Guidance, Control, and Dynamics*, Vol. 26, No. 2, 2003, pp. 375–379.
doi:10.2514/2.5059

[27] Hartl, R. F., Sethi, S. P., and Vickson, R. G., "A Survey of the Maximum Principle for Optimal Control Problems with State Constraints," *SIAM Review*, Vol. 37, No. 2, 1995, pp. 181–218.
doi:10.1137/1037043

[28] Umehara, H., and McInnes, C. R., "Fuel-Optimum Near-Miss Avoidance Control for Clustered Satellites," *Proceedings of the 18th International Symposium on Space Flight Dynamics*, ESA SP 548, Paris, 2004, pp. 1093–1094.

[29] Bartholomew-Biggs, M. C., "A Penalty Method for Point and Path State Constraints in Trajectory Optimization," *Optimal Control Applications and Methods*, Vol. 16, Nos. 1–4, 1995, pp. 291–297.

[30] Teo, K. L., and Jennings, L. S., "Nonlinear Optimal Control Problems with Continuous State Inequality Constraints," *Journal of Optimization Theory and Applications*, Vol. 63, No. 1, 1989, pp. 1–22.
doi:10.1007/BF00940727

[31] Graichen, K., and Petit, N., "Constructive Methods for Initialization and Handling Mixed State-Input Constraints in Optimal Control," *Journal of Guidance, Control, and Dynamics*, Vol. 31, No. 5, 2008, pp. 1334–1343.
doi:10.2514/1.33870

[32] Hermant, A., "Homotopy Algorithm for Optimal Control Problems with a Second-order State Constraint," *Applied Mathematics and Optimization*, Vol. 61, No. 1, 2010, pp. 85–127.
doi:10.1007/s00245-009-9076-y

[33] Bertsekas, D. P., "Necessary and Sufficient Conditions for a Penalty Method to be Exact," *Mathematical Programming*, Vol. 9, No. 1, 1975, pp. 87–99.
doi:10.1007/BF01681332

[34] Han, S. P., and Mangasarian, O. L., "Exact Penalty Function in Nonlinear Programming," *Mathematical Programming*, Vol. 17, No. 1, 1979, pp. 251–269.
doi:10.1007/BF01588250

[35] Gonzaga, C. C., and Castillo, R., "A Nonlinear Programming Algorithm based on Non-coercive Penalty Functions," *Mathematical Programming*, Vol. 96, No. 1, 2003, pp. 87–101.
doi:10.1007/s10107-002-0332-z

[36] Pillo, G. D., and Grippo, L., "Exact Penalty Functions in Constrained Optimization," *SIAM Journal on Control and Optimization*, Vol. 27, No. 6, 1989, pp. 1333–1360.
doi:10.1137/0327068

[37] Liuzzi, G., and Lucidi, S., "A Derivative-Free Algorithm for Inequality Constrained Nonlinear Programming via Smoothing of an ℓ_∞ Penalty Function," *SIAM Journal on Optimization*, Vol. 20, No. 1, 2009, pp. 1–29.
doi:10.1137/070711451

[38] Smith, S., and Mayne, D. Q., "Exact Penalty Algorithm for Optimal Control Problems with Control and Terminal Constraints," *International Journal of Control*, Vol. 48, No. 1, 1988, pp. 257–271.
doi:10.1080/00207178808906173

[39] Mayne, D. Q., and Polak, E., "An Exact Penalty Function Algorithm for Optimal Control Problems with Control and Terminal Equality Constraints, Part 1," *Journal of Optimization Theory and Applications*, Vol. 32, No. 2, 1980, pp. 211–246.
doi:10.1007/BF00934725

[40] Mayne, D. Q., and Polak, E., "An Exact Penalty Function Algorithm for Optimal Control Problems with Control and Terminal Equality Constraints, Part 2," *Journal of Optimization Theory and Applications*, Vol. 32, No. 3, 1980, pp. 345–354.
doi:10.1007/BF00934557

[41] Tschauner, J., and Hempel, P., "Optimale Beschleunigeungsprogramme fur das Rendezvous Manover," *Astronautica Acta*, Vol. 10, Nos. 5–6, 1964, pp. 296–307.

[42] Alfriend, K. T., Vadali, S. R., Gurfil, P., How, J. P., and Breger, L., *Spacecraft Formation Flying: Dynamics, Control and Navigation*, Elsevier, Oxford, U.K., 2010, pp. 103–117.

[43] Gurfil, P., "Relative Motion Between Elliptic Orbits: Generalized Boundedness Conditions and Optimal Formationkeeping," *Journal of Guidance, Control, and Dynamics*, Vol. 28, No. 4, 2005, pp. 761–767.
doi:10.2514/1.9439

[44] Bertrand, R., and Epenoy, R., "New Smoothing Techniques for Solving Bang–Bang Optimal Control Problems: Numerical Results and Statistical Interpretation," *Optimal Control Applications and Methods*, Vol. 23, No. 4, 2002, pp. 171–197.
doi:10.1002/oca.709

[45] Bourbaki, N., *Topological Vector Spaces, Elements of Mathematics*, Springer–Verlag, Berlin, 1987, Chaps. 1–5.

[46] Pareschi, G., and Ferrando, P., "The SIMBOL-X Hard X-ray Mission," *Experimental Astronomy*, Vol. 20, Nos. 1–3, 2005, pp. 139–149.
doi:10.1007/s10686-006-9062-1

[47] Cesari, L., *Optimization–Theory and Applications, Problems with Ordinary Differential Equations*, Springer–Verlag, New York, 1983, pp. 303–318.

[48] Aubin, J. -P., and Cellina, A., *Differential Inclusion*, Springer–Verlag, New York, 1984, p. 13.